eprints@whiterose.ac.uk
https://eprints.whiterose.ac.uk/

Multicomponent Fuel Droplet Combustion Investigation Using Magnified High Speed Backlighting and Shadowgraph Imaging

Ahmad Muneerel-Deen Faik[1], Yang Zhang[2]

[1]Mechanical Engineering Department, Al-Mustansiriyah University, Baghdad, Iraq

[2] Department of Mechanical Engineering, The University of Sheffield, Sheffield, UK

Abstract

The liquid-phase processes occurring during fuel droplet combustion are important in deciding the behaviour of the overall combustion process, especially, for the multicomponent fuel droplets. Hence, understanding these processes is essential for explaining the combustion of the multicomponent fuel droplet. However, the very fast combustion of the too small fuel droplet makes experimental investigation of these processes uneasily affordable. In the present work, a high speed backlighting and shadowgraph imaging of the multicomponent fuel droplet combustion including liquid-phase dynamics are performed. Two categories of multicomponent fuels – in which diesel is the base fuel – are prepared and utilized. The first category is biodiesel/diesel and bioethanol/diesel blends, while the second category is the water-in-diesel and diesel-in-water emulsions. Specific optical setups are developed and used for tracking droplet combustion. The first setup is associated with the backlighting imaging with the resulting magnification of the droplet images being 30 times the real size. The second optical setup is used for shadowgraph imaging, with the resulting magnification being 10 times the real size. Using these setups, spatial and temporal tracking of nucleation, bubble generation, internal circulation, puffing, microexplosion, and secondary atomization during the combustion of isolated multicomponent fuel droplets are performed. Spatial and temporal tracking of the sub-droplets generated by secondary atomization, and their subsequent combustion, in addition to their overall lifetimes have also been performed. Accordingly, a comparison of the burning rate constant between the parent droplet and the resulting sub-droplets is carried out. The rate of droplet secondary atomization is higher than those obtained by relatively low imaging rate. Additionally, it is shown that during a large portion of its entire lifetime, the droplet geometry has been affected by combustion significantly.

Keywords: Multicomponent fuel, Blends, Emulsions, Droplet liquid-phase, Nucleation, Puffing, Secondary atomization

1.1 Introduction

A large portion of the global energy requirements comes from burning liquid hydrocarbons. This is due to the ease and flexibility of transporting and storing these fuels compared to the gaseous forms, in addition to their availability compared to the solid fuels. Liquid fuel combustion consists mainly of four processes, namely: atomization and droplet formation, droplet fuel evaporation, combustible mixture formation, and mixture combustion [1]. Atomization and droplet formation is important in combustion, since most of the combustion systems (such as the industrial furnaces and internal combustion engines) work on liquid fuels that cannot be used before being atomized. And it is essential in increasing the combustion efficiency in such systems because of the high liquid surface to mass ratio generated after atomization, which in turn leads to higher rates of evaporation and mixing, and then combustion [2]. Some of these liquid fuels are utilized in the form of multicomponent fuels or fuel mixtures. This is either for increasing the performance of the combustion system by the addition of higher heating value fuels, or reducing the harmful environmental impact of the conventional fuels, or because of the depletion of the conventional liquid fuel resources. In the multicomponent fuel mixtures, no chemical reaction will occur between the fuel constituents, and each constituent sustains its own physical and chemical properties. Therefore, the combustion of the resulting mixture is more complicated than that of the neat fuel because different components are burning simultaneously at the same point and instant of time. Hence, unlike the single component fuel droplet combustion – in which droplet evaporation is the rate controlling process – the multicomponent fuel droplet combustion encompasses the effect of droplet interior heat and mass transfer [3]. As a result, the multicomponent fuel droplet combustion is much more complicated compared to the single-component droplet combustion. Firstly, the different constituents of the multicomponent fuel have different boiling points and different evaporation rates that leads to creating concentration gradients inside the droplet (in the liquid phase). Secondly, due to the boiling point gradient, a difference in volatility tendency is expected. Hence, the more volatile components tend to evaporate first until their concentrations are reduced, changing the concentration gradient inside the droplet. Lastly, the evaporation of the more

volatile components reduces their concentrations but does not consume them completely. Thus, the remaining quantities of the highly volatile components tend to diffuse to the droplet surface due to their tendency of evaporation, and the less volatile components will tend to diffuse inward. This in turn, will create an internal circulation in the liquid phase, and will affect the evaporation rate of the droplet because of concentration difference on its surface along its lifetime [4]. Accordingly, droplet combustion of the multicomponent fuels has been and being investigated extensively both theoretically and experimentally for better understanding of the physical and chemical processes associated with this form of droplet combustion [3,5–7]. Besides, different physical processes which are associated with the combustion of multicomponent fuel droplets have been the scoop of different studies, such as the puffing and microexplosion leading to droplet secondary atomization. These processes are initiating and occurring in the liquid-phase of the fuel droplet either in the surface or deep within the droplet internals, and are directly affecting the overall droplet combustion behaviour. Droplet microexplosion is defined as the prompt fragmentation of the multicomponent droplet as a result of nucleation and explosive boiling of the less boiling point component(s) [8,9]. If this fragmentation is less intensive and limited to part of the droplet, it is usually called as puffing. Though, Tsue et. al. [10] and Watanbe et al., [11], gave a more specific definition for droplet puffing, that is the process of vapour jet liberation form the surface of the multicomponent fuel droplet. This vapour jet is usually filled with finely small sub-droplets of the dispersed phase. The continuous phase may also detaches from the droplet surface in the form of ligaments or small size droplets as a consequence of an intensive puffing incident [12]. This detachment of ligaments and small droplets is called secondary atomization. Therefore, the secondary atomization is defined as the processes of droplet disintegration into smaller size droplets. This disintegration results when the dynamic forces acting on the droplet are higher than the restoration force of the droplet [13]. Puffing and microexplosion are direct results of the nucleation and bubble generation within the multicomponent fuel droplets. The occurrence of these processes during the multicomponent fuel droplet combustion is firstly described by Lasheras and co-workers [14–16] who gave a general name for these processes that is the *disruptive burning* of the multicomponent fuel droplets. The same has been distinguished by Avedisian and co-workers [17–19] for n-heptane based binary fuel mixtures including emulsions. Hoxie, Schoo, and Braden [7], and Botero et al., [6] have also described the occurrence of disruptive burning during the combustion of

soybean oil/butanol, and diesel/ethanol/biodiesel blend droplets respectively. Lasheras, Fernandez-Pello, and Dryer [15] studied the disruptive burning of the ethanol/n-paraffin and n-propanol/n-paraffin binary solutions under atmospheric pressure. They found that droplet disruption results from the homogeneous bubble nucleation, expansion, and explosion inside the droplet. The occurrence of nucleation within the burning droplet has been reported by Lasheras et. al., [14,15] during the combustion of binary n-paraffin mixtures. They have detected droplet size increase during droplet combustion and attributed it to the bubble formation. Chung and Kim [20] have also attributed the water sub-droplets increase within a water-in-dodecane emulsion droplet evaporating on a hot surface to the formation of water bubbles. They have detected the water sub-droplet increase by comparing droplet microscope images before and after heating. Wang, Liu, and Law [3] have also conceived bubble nucleation inside freely falling, burning, multicomponent fuel droplets, and evaluated the bubble growth rate and the bubble to droplet size ratio. Tsue et. al., [21] have imputed the microexplosion occurrence to the formation of water vapour bubbles inside the burning droplets of n-dodecane-in-water and n-tetradecane-in-water emulsions. Wang et. al., [22] have spotted heterogeneous nucleation occurrence as a result of trapped air bubbles inside the collision-merging methanol/alkane droplets. These air bubbles serve as nucleation sites inside the droplet. A more comprehensive theoretical description of the nucleation and bubble formation within emulsion fuel droplets is given by Shinjo et. al., [9,23,24]. They have shown that droplet puffing is the result of bubble growth inside the droplet. Bubble burst at the droplet surface has also been described, and the effect of initial locations of the boiling bubble and the dispersed phase sub-droplet on the bubble burst intensity has also been evaluated. In conclusion, a substantial number of studies have been conducted to explain the physics of puffing, secondary atomization, and microexplosion. As a result, the effects of these processes on the combustion efficiency by enhancing fuel evaporation and fuel/air mixing are well addressed. Additionally, the effect of nucleation and bubble growth in the droplet liquid-phase on the initiation and development of these processes is also established and deduced with respect to droplet size increase. However, except the numerical simulation work performed by Shinjo et al., bubble nucleation initiation, growth, and its subsequent dynamics inside the burning multicomponent fuel droplet has not been well investigated. In particular, magnified experimental investigation of the droplet liquid-phase dedicated for studying bubble nucleation is not available. Hence, further comprehension of the physics of these processes including initiation and

development is required. This can be executed by conducting a magnified experimental visualization and tracking of the droplet liquid-phase for obtaining in-depth quantitative and qualitative description of these processes and the corresponding mechanisms. Therefore, the present work is dedicated to fulfil this objective, and in turn, offer experimental description of the aforementioned processes.
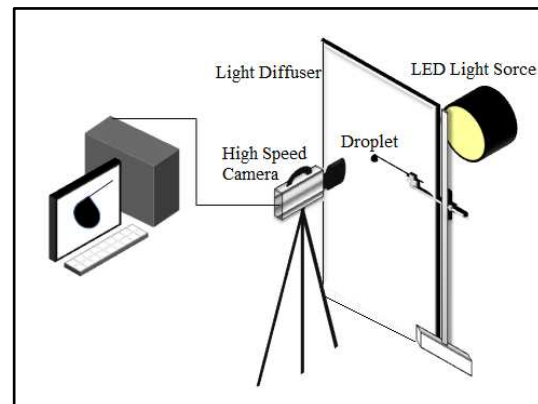
1.2 Experimental Work

1.2.1 The Multicomponent Fuel Preparation

The water-in-diesel (WD) and diesel-in-water (DW) emulsions have been prepared in the lab prior to the combustion experiments. Since emulsions are mixtures of two (or more) insoluble liquids, they are thermodynamically unstable. Consequently, producing a long-lasting emulsion requires a third agent that accumulates at the interface between the two liquids forming the emulsion; this agent is the *emulsifier (or surfactant)*. The rule of the emulsifier is to form protective, elastic, and relatively strong film layer that can withstand droplet collision and prevent phase separation. However, the type of emulsifier is an essential parameter in defining the type of emulsion. Hydrophilic emulsifiers prompt the formation of oil-in-water emulsions, while water-in-oil emulsions are mostly produced by the use of lipophilic emulsifiers [25]. This is known as *Bancroft's Rule* which states that "*the phase in which the surfactant is more soluble is the continuous phase*" [26]. This solubility inclination is characterized by the Hydrophile-Lipophile Balance (HLB) number. The HLB number is developed by Griffin as the balance of the size and strength of both the hydrophilic and lipophilic groups within the emulsifier molecules [27]. Hence, each emulsifying agent has its own HLB number which is in the range of 0 to 20, and this number defines whether the emulsifier is oil-soluble ($0 \leq$ HLB ≤ 9), water-soluble ($11 \leq$ HLB ≤ 20), or hydrophilically-lipophilically balanced (HLB $= 10$). Accordingly, in the present work two emulsifiers have been selected for emulsion preparation. The first is the Polysorbate 80 (HLB = 15) for making the diesel-in-water emulsions, and the other is the Sorbitan Mono Oleate (also known as Span 80) (HLB = 4.3) for making the water-in-diesel emulsions. The method followed and described by Califano, Calabria, and Massoli [28] and Jackson and Avedisian [18] has been used for preparation. For each of the emulsions, the emulsifier is added to the continuous phase (diesel in the case of water-in-diesel emulsions, and water in the case of diesel-in-water emulsions) with a quantity less than 1% of the mixture volume. The emulsifier and the continuous phase are then stirred for ensuring solubility. The required quantity of the dispersed phase (water in the case of water-in-diesel emulsions, and diesel in the case of diesel-in-water emulsions) is then added gradually to the mixture. A 20000 rpm electric hand blender has been used for mixing the liquids for more than five minutes until a homogeneous milky white liquid is produced. Water content in both emulsions has been fixed at 10%, 20%, and 30% of the total emulsion volume, and the remaining part is diesel. Finally, it is worthy to mention that for every new test, a new emulsion sample is prepared and tested. Hence, these samples are kept in a small glass container, and during the testing period no visible changes have been observed. While, the biodiesel-in-diesel (BD) and ethanol-in-diesel (ED) blends have been prepared in-lab. For each blend, three blending proportions are used, in which diesel accounts for (90%, 80%, and 70%) of the total mixture volume, and the added fuel accounts for the remaining (10%, 20%, and 30%) respectively. These proportions are selected in accordance to those corresponding values of diesel emulsions. This ensures relatively comparable results.

1.2.2 Optical Setups

Two optical setups have been developed for studying droplet combustion simultaneously. The first setup is based on the backlighting imaging technique and its schematic diagram is shown in Figure 1. The droplet is suspended on a (100 μm) monofilament single SiC fibre. This fibre is attached to the sliding arm of a lab stand for easier control of the droplet position in accordance to the camera.

Figure 1: Experimental setup of the droplet combustion with backlighting imaging.

The optical setup is an integration of a Photron SA4 high speed camera and a Nikon AF Micro NIKKOR 60mm f/2.8D lens with a 55mm macro extension tube set that is placed between the camera and lens. The high speed camera is set in front of the droplet, whereas an IDT 19-LED high intensity illuminator is installed behind the droplet serving for providing the light required for illumination. A translucent white light diffuser is

installed between the droplet and the light source for lower light intensity, and more uniform light distribution behind the droplet. The camera is set to 40000 fps framing rate, 25µs exposure time, and 320x240 pixels image resolution. The area covered by the camera was 3.2x2.4 mm^2, giving a spatial resolution of 10 µm/pixel for each image. The magnification rate achieved using this setup is 30 times the physical size.
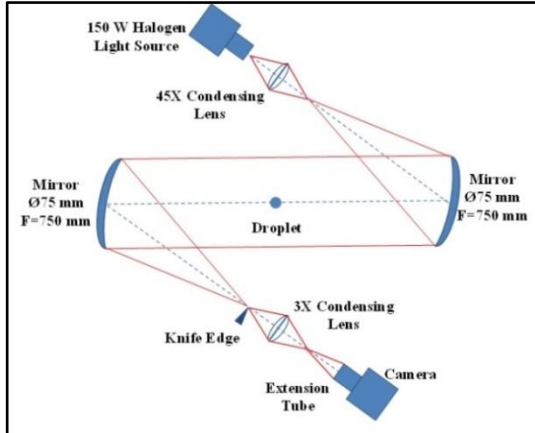

Figure 2: Schematic of the schlieren imaging setup.

Figure 2 shows the general setup of the Z-type shadowgraph arrangement used in the second imaging method. In this setup, the light coming from the halogen light source is focused and magnified by the 45x condensing lens before reaching the first mirror, and focused again by the 3x condensing lens after passing the second mirror. The high speed camera is set to 10000 fps framing rate, 100 µs exposure time, and 384x288 pixels image resolution. The area covered by the camera was 9.6x7.2 mm^2, giving a spatial resolution of 40 µm/pixel for each image. The magnification rate achieved using this setup is 10 times the physical size without any on-screen magnification. Hence, a detailed investigation of the instantaneous puffing and secondary atomization, and the consequent droplet shape variation during the overall combustion period is achieved. The images have been stored in the (TIFF) format and processed using specially written Matlab algorithms. The time periods on the droplet images are expressed in terms of droplet lifetime, otherwise, the starting point will be stated.

1.3 Results and Discussions

Generally, the droplets of all the multicomponent fuel mixtures studied in the present work have experienced puffing and secondary atomization. The puffing incidents are shown to occur over the entire droplet lifetime. The number and intensity of these puffs are variable for each type of the multicomponent fuel mixtures. The biodiesel/diesel blends have shown the least

number of puffs compared to the other mixtures that were relatively comparable to each other. Furthermore, some of the water-in-diesel and diesel-in-water emulsion droplets have suffered microexplosion before undergoing complete evaporation. This in turn, have resulted in the emulsion droplets experiencing high number of puffs along a short period of time, resulting in higher puffing rates compared to the droplet of the biodiesel/diesel and ethanol/diesel blends.
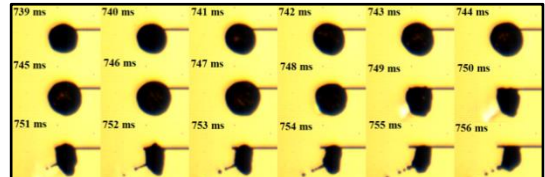
Figure 3: Temporal sequence of an ED20 droplet size change before and during puffing.

Additionally, despite the type of fuel mixture, almost all the droplets shared the same sequence of events before and during puffing. These events are shown in Figure 3 for puffing from an ED20 fuel droplet. The first sign of puffing occurrence is the droplet size increase as shown in the images corresponding to time periods 741 ms to 747 ms in Figure 3 compared to time periods 739 ms and 740 ms. This increase in diameter is evaluated to be from 1.5 mm on 739 ms to 1.8 mm on 747 ms, which means about 20% of the droplet instantaneous diameter. This droplet size increase is attributed to the bubble growth inside the droplet prior to puffing [29,30]. This bubble continues pushing the thin layer of the droplet surface outwards from inside until the moment when the droplet surface cannot withstand this force, so the droplet raptures locally and the vapour contained in the bubble emerges outside in the form of a jet as shown by the white spray emerging from the droplet in Figure 3 images 748 ms to 750 ms respectively. The release of the vapour from the droplet causes sudden size reduction and shape deformation of the burning droplet as shown in images 749 ms to 756 ms compared to images 741 ms to 747 ms. To this point, vapour ejection by puffing is complete. However, different processes will take place within the droplet subsequent to the puffing incident according to the puffing strength [24]. If the puff is weak, the droplet will retain its original shape and size after a short period of recoiling. But, if the puff is strong, ligament detachment from the droplet surface leading to sub-droplet generation will take place as shown in images 751 ms to 756 ms in Figure 3 for the ED20 fuel droplet, and Figure 4 for the WD10 fuel droplet. In the former, the puffing occurrence gave rise to four sub-droplets that are ejected from the droplet subsequently, whereas in the latter, many sub-droplets are generated and emitted away from the droplet as a result of a strong puff. It should be

emphasised here that prior to sub-droplet ejection, the parent droplet is found to encounter a certain shape change that may be linked to the strength of the puff and in turn, to the size of the bubble triggering that puff. An example of this shape variation is shown in Figure 4 (image 0.8 ms and the followings).
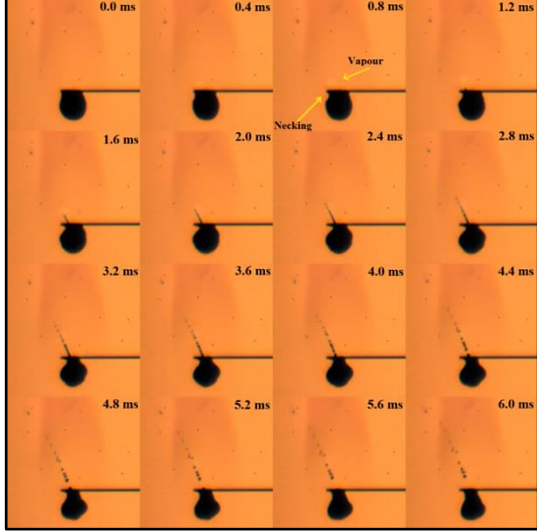

Figure 4: WD10 droplet necking prior to puffing and the resulted multiple sub-droplets subsequent an intense puffing incident.

As shown in these images, droplet necking takes place on the droplet/fibre contact region, this necking occurred just after the vapour release. This implies that this necking is a result of the vacuum created on the droplet section near its surface due to vapour release by puffing. To fill up this vacuum and to compensate for the released vapour, droplet edges moved inwards creating this neck. This necking and inward movement may enhance sub-droplet evolution from the parent droplet by the impact of the oppositely moving droplet edges in one hand, and the decrease in sub-droplet ejection area and the resulting increase in the ejection velocity in the other hand. The effect of this necking can be shown by the relatively large number of sub-droplets emerged from the parent droplet during the same puffing incident.

Figure 5 shows the temporal sequence of flame blow-off during the combustion of a DW10 fuel droplet. Flame blow-off has been clearly revealed using shadowgraphy. However, due to the low light intensity of the shadowgraph imaging, the images have been processed for better demonstration of the phenomenon. Hence, the images in Figure 5 are the processed form of the original images showing the droplet in blue colour and the flame in yellow. Thus, from Figure 5, the flame is firstly close to the droplet surface as shown in images 360.7 ms and 361.6 ms. Then, due to the effect of the vapour jet released by puffing from the droplet surface, the visible flame (or soot) segment that is the nearest to

the droplet moves away from the droplet creating a gap with the latter as shown in images 362.6 ms and the followings. The height of this gap depends on the intensity and penetration of the vapour jet, and it has been evaluated for the case shown in Figure 5 and found to be 2.5 mm from the position of the fibre. This gap decreased again and soot accumulation resumed once the effect of the vapour is vanished. This visible flame blow-off phenomenon has been found to occur during the combustion of the water-in-diesel and diesel-in-water emulsion droplets rather than the biodiesel/diesel and ethanol/diesel blends. This suggests that the intensity of the puffs resulting from the emulsion droplets is higher than those of the corresponding blend droplets.
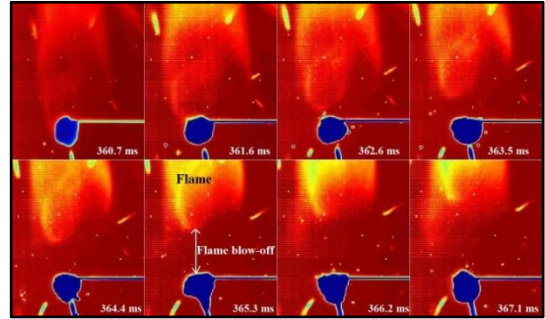
Figure 5: Flame blow-off subsequent to vapour jet puffing from a DW10 droplet.

Furthermore, the maximum penetration of the vapour jet is found to be variable, and is a function of the size of the growing bubble within the droplet [12]. This penetration is expressed in terms of the droplet instantaneous radius prior to puffing, and is found to range from a fraction of the droplet radius to several droplet radii. Hence, for characterizing the puffing intensity of the multicomponent fuel mixtures during droplet combustion, the average penetration distance of the vapour jet emerged by droplet puffing is calculated. Another advantage of the vapour penetration calculation is that it describes more the puffing intensity rather than the number of puffs per droplet lifetime. This is because as mentioned earlier, the difference in droplet lifetime between the blends and emulsions – due to emulsion droplets microexplosion – and the difference in droplet instantaneous diameter will result in a non-realistic description of the puffing rate. Additionally, the calculated puffing rate will not be practically worthwhile because, the real droplets in the liquid fuel sprays are order of magnitudes less than the ones studied in the present work, in addition to the lifetime of the real droplet is much less than that of the one studied in-lab. Hence, it is more practically beneficial to evaluate the effect of these puffs firstly, on the neighbouring droplets, and secondly, on the overall spray configuration. Hence the average effective distance – or penetration – of these puffs has been evaluated
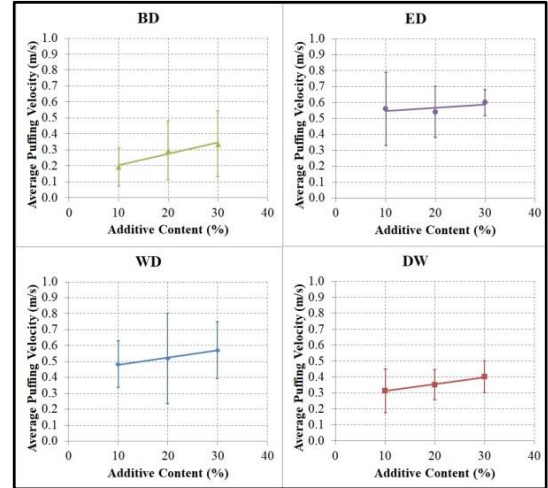
5

for all the multicomponent fuels and shown in Figure 6 against the concentration of the added components (water, biodiesel, and ethanol) to the overall mixture volume.
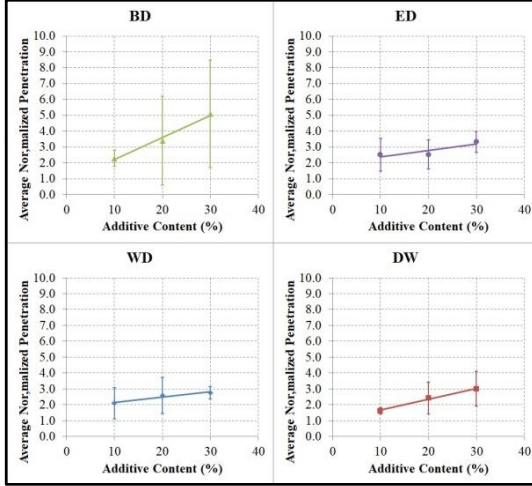
Figure 6: The effect of water, biodiesel, and ethanol concentrations on the puffing vapour penetration.

The vapour jet penetration is normalized by the droplet instantaneous radius to give a non-dimensional characterization of the distance. The presented penetration in Figure 6 is the average value of all the puffs for each fuel droplet. The average puffing velocity, on the other hand, has been evaluated by dividing the max penetration in millimetre by the total time required in millisecond. The average of all the velocity values calculated from every puffing incident has been evaluated and presented for every multicomponent fuel. As shown in Figure 6, the average normalized penetration is proportional to the concentration of the added component (whether it is water, biodiesel, or ethanol), so it is increasing by the increase of additive concentration in the fuel mixture for both blends and emulsions. The uncertainty of these values has also been examined by evaluating the standard deviation of the calculated penetrations. As shown in the figure, except the BD results, the standard deviations of all the multicomponent fuels are quiet small suggesting highly repeatable results. Additionally, it may be implied from Figure 6 that the BD blend droplets are the ones with the highest penetration and the DW emulsion droplets are the ones with the lowest. In fact, the BD droplets are shown to have the lowest puffing rate among all the multicomponent fuels. But, what is shown by Figure 6(a) is the vapour penetration normalized by the droplet instantaneous diameter as mentioned earlier. So, in the case of the BD droplets, firstly the droplet undergoes complete evaporation, and secondly, the puffs take place at the final stages of the droplet lifetime when the droplet diameter is relatively small. Therefore, the resulting penetration to droplet diameter is comparatively high. This is exactly the opposite scenario in the case of the DW

droplets. The DW droplet consistently explodes before complete evaporation, and the puffing takes place with the droplet instantaneous diameter is relatively large, so that the resulting normalized penetration is slightly small. The WD emulsions and ED blends on the other hand, have experienced both situations, where complete evaporation takes place in both mixture droplets, and puffing rate is higher and it occurs slightly earlier than that of the BD droplets.


Figure 7: The effect of water, biodiesel, and ethanol concentrations on the average puffing velocity.

Figure 7 shows the velocity of the vapour jet ejected by puffing from the multicomponent fuel droplets during combustion. This vapour jet velocity is presented against the concentration of the added components (water, biodiesel, and ethanol) to the overall mixture volume. Figure 7 interprets well the real puffing condition, where the WD and ED puffs are faster than those resulting from the DW and BD droplets. As shown by the figure, the average vapour ejection velocity is also increasing with the increase of additive concentration in the multicomponent fuel mixture for all the fuels. As mentioned earlier, this velocity is evaluated according to the total time required by the vapour jet to reach its maximum penetration. However, the initial discharge velocity has also been evaluated and its values are found to be ten times the average velocity shown in Figure 7. These calculated velocity ranges are in agreement with the 5 m/s discharge velocity reported by Miglani, Basu, and Kumar [12] for water-ethanol mixtures, but less than the predicted values by Shinjo et. al., [24] for the velocity of a vapour emerging from a decane/ethanol droplet. The obtained values for the ethanol/diesel droplets – which are the most comparable mixtures to the decane/ethanol mixture – are in the range of 0.5 to 0.6 m/s whereas the reported value is about 2 m/s and the discharge velocity is 20 m/s. This discrepancy in values between what is predicted and what is calculated experimentally could be attributed to the

6

penetration true value issue raised above, since the evaluated penetration values should be divided by the sine of the inclination angle for obtaining the true values of the puffing penetration distance.

### 1.3.1 Sub-Droplet Emission by Secondary Atomization

Figure 8 shows the temporal sequence of sub-droplet emission from a BD10 fuel droplet during combustion. This sub-droplet is produced subsequent to droplet recoiling after puffing.
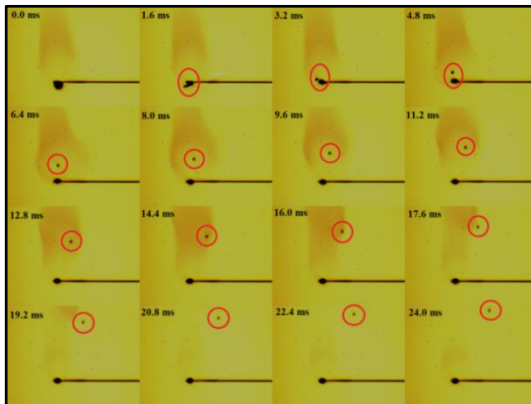
Figure 8: Temporal sequence of sub-droplet emission from a burning BD10 droplet.

The size of the sub-droplet is found to be 0.2 mm whereas the size of the parent droplet prior to secondary atomization is 0.42 mm. The trajectory of the sub-droplet is tracked by the aid of image processing using Matlab. Using the length of this trajectory and the time required for the sub-droplet to pass it, the flow velocity of the sub-droplet is evaluated and found to be 0.26 m/s which is in the same range with the puffing velocity of the vapour jet shown in Figure 7 for BD10. Additionally, sometimes multiple sub-droplets are ejected from the droplet surface at the same time. However, the size and velocity of the emerging sub-droplets are not necessarily the same. Sometimes, the emerging sub-droplet is entirely small so that it will evaporate completely once ejected from the droplet surface, such as the sub-droplets emerging from the WD10 fuel droplet shown in Figure 4. While, in some instants, the sub-droplet is quite large in size so that it may ignite before undergoing complete evaporation, and in some extreme cases, it may withstand its own surrounding flame for a period of time. However, despite the fact that the parent droplets under investigation are larger than the real spray droplets. The number of sub-droplets gives an indication of the tendency of the fuel to secondary atomization. Therefore, an algorithm has been developed for counting the number of sub-droplets emitted per incident and the occurrence time, and then the total number of these sub-droplets from the shadowgraph images of the droplets undergoing combustion.

Figure 9 shows the total number of sub-droplets ejected during the overall droplet lifetime for the water-in-diesel and diesel-in-water emulsions, in addition to the biodiesel/diesel and ethanol/diesel blends at all the three proportions 10%, 20%, and 30% additive concentration in the overall mixture volume. As the figure shows, a relatively large variation of the total sub-droplets number is obtained between the four fuel mixtures. Therefore, a logarithmic scale is used for presenting the data in a more comparable configuration. It can be seen from the figure that the number of sub-droplets generated by secondary atomization is proportional to the concentration of both water and biodiesel in the cases of WD emulsions and BD blends, while it is inversely proportional to the water and ethanol concentrations for the DW emulsions and ED blends respectively. This secondary atomization is an indirect consequence of the nucleation inside the droplet [24]. Bubble nucleation inside the droplet leads to puffing, and puffing is often followed by secondary atomization.
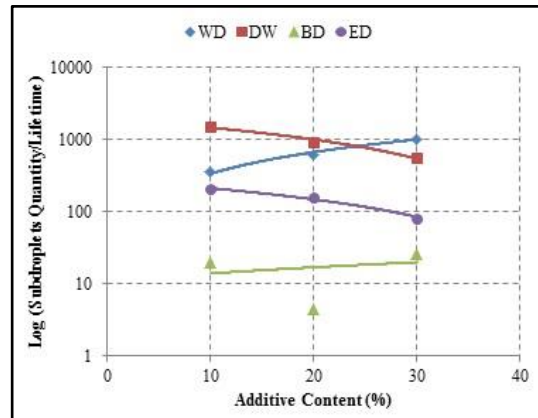

Figure 9: The effect of additive concentration on the number of sub-droplets emitted during droplet lifetime.

Hence, the change in the mixtures trend for secondary atomization may be associated to the bubble nucleation and growth rates within the droplet. It can be noticed also, that despite the difference in values between the mixtures, some similarity in trends is obtained between two pairs of them. The sub-droplets number in the WD emulsions and the BD blends is shown to increase by increasing the concentrations of both water and biodiesel respectively in the mixture. Exactly the opposite is noticed to occur for the DW emulsions and the ED blends. These different behaviours are sequentially explained. Firstly, regarding the BD blends, both diesel and biodiesel have relatively high boiling points and these boiling points are close to each other despite that of the biodiesel is higher than the boiling point of the diesel. This low boiling point difference between the BD blend components is not available for the ED, WD, and DW fuel mixtures; therefore, they have experienced higher rates of secondary atomization compared to

the BD blends. It is established on the other hand, that the nucleation and bubble growth rate within the liquid-phase of the multicomponent fuel mixture is a function of the boiling point difference between the different components of the mixture [14]. Therefore, this low boiling point difference resulted in lower nucleation rates within the BD fuel droplets and in turn, lower secondary atomization rates. Additionally, the nucleation rate inside the multicomponent fuel droplet is influenced by the density ratio between the dispersed phase and the continuous phase. The bubble nucleation and growth rate within the droplets of the multicomponent fuel mixtures depends on the densities of the constituents forming the mixture [31]. This is because bubble growth from a higher density liquid to a lower density liquid is certainly different from bubble growth from lower density component to a higher density component. Bubble growth towards the lower density component suggests higher nucleation and growth rates due to the less resistance to the bubble growth, while bubble growth towards the higher density components is suggesting a decrease in the nucleation rate because of the increased resistance to the bubble growth due to the high density of the liquid. Thus for the BD blends, biodiesel is the higher density and higher boiling point component, while diesel is the lower density and lower boiling point component. Hence, it is expected that the diesel is the constituent undergoing superheated boiling and nucleation, and that bubble growth will take place from diesel to biodiesel. This means bubble growth towards a higher density liquid, suggesting a relatively low rate of nucleation. However, increasing the biodiesel concentration in the blend increased the secondary atomization rate, implying a higher nucleation rate, which is true, but this increased rate of secondary atomization is attributed to increasing the nucleation sites within the droplet by increasing the biodiesel concentration due to the increase in the interference regions between diesel and biodiesel. Secondly, regarding the secondary atomization in the ED blends, the scenario is slightly different from that of the BD blends. The boiling point of ethanol is much less than that of diesel and the density also is slightly lower. Therefore, in the case of a burning ED fuel droplet, it is expected that ethanol will ignite first due to its higher volatility and lower boiling point, resulting that the diesel will suffer the superheated boiling as in the case of the BD blends. But, the density of ethanol is less than that of the diesel; therefore, nucleation and bubble growth is higher due to the lower resistance of the ethanol to bubble nucleation. This high growth rate within the ED droplets is reflected on the size of the sub-droplets ejected from the parent droplet, the majority of these sub-droplets are of relatively large sizes – in fact they are the largest among the other

fuel mixtures – so they are more in the form of large ligaments rather than small sub-droplets as shown in Figure 10.
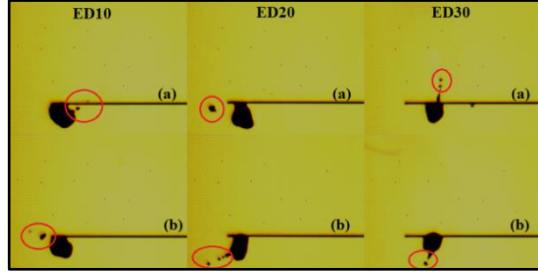
Figure 10: Sample images of the large sub-droplets ejected from the ED fuel droplets.

Moreover, it is noticed that increasing the ethanol concentration in the blend resulted in a slight change in the sub-droplet ejection behaviour of the droplet. For the ED10 droplets, multiple sub-droplets are ejected per single incident. The number of these sub-droplets is shown to decrease and their sizes increase when the ethanol concentration is increased. Therefore, in the ED30 case, a single, large sub-droplet is ejected per incident rather than multiple, small sub-droplets. Thus, the number of sub-droplets is shown to be inversely proportional to the ethanol concentration on Figure 9. Thirdly, regarding the WD and DW emulsions, both of the emulsions have experienced a significant increase in the sub-droplet ejection processes. This suggests higher nucleation rates compared to the BD and ED blends. This high nucleation rate of the emulsions compared to the blends has also been described by Lasheras, Fernandez-Pello, and Dryer [14] and is attributed to the large specific volume change of water in the emulsion droplet compared to the components of the blends, in addition to the wide dispersion of water droplets in the emulsion mixture compared to the blends, this in turn, results in higher number of nucleation sites initiation within the emulsion mixture at the same time compared to the blends. These two main parameters led to higher nucleation rates and consequently higher secondary atomization rates from the water-in-diesel and diesel-in-water emulsion droplets compared to the biodiesel/diesel and ethanol/diesel blends. Nevertheless, increasing the water concentration in the emulsions had different effects on the rate of sub-droplet generation from both the WD and DW emulsions as shown in Figure 9. The sub-droplet emission rate is shown to increase in the WD emulsions and decrease in the DW emulsions with increasing the water concentration. Sub-droplet generation rate escalation due to increasing the water concentration is expected because of augmenting the nucleation sites by increasing water droplets in the emulsion. But, the decrease in sub-droplet generation shown in the DW emulsions is the unexpected behaviour. This could be attributed to the effect of surfactant used

8

for emulsion preparation. Because the type of surfactant is the only difference between the WD and DW emulsions, especially with the volume fractions of the constituents are the same. The effect of surfactant weakens with the increase of the emulsion temperature [21]. Therefore, water/diesel separation, and in turn, water coagulation in the centre of the droplet will take place making the droplet to burn in a single-component-like mode rather than multicomponent combustion. This water coagulation is expected to escalate by increasing the water concentration in the emulsions because the same quantity of surfactant is used for all the emulsions, hence, its effect is decreasing with the increase of water volume because of the increased interfacial regions within the emulsion droplet by the increase of water concentration. This water coagulation, then, is the effective parameter in decreasing the number of sub-droplets generation due to nucleation rate decrease [32]. This water coagulation is more revealed during the droplet microexplosion analysis in the next section. However, explosive boiling in the heart of the droplet will continue to occur due to the availability of water. The same trends of Figure 9 are shown in Figure 11 which illustrates the effect of added liquid (water, biodiesel, and ethanol) concentrations on the net portion of secondary atomization time compared to the overall droplet lifetime.
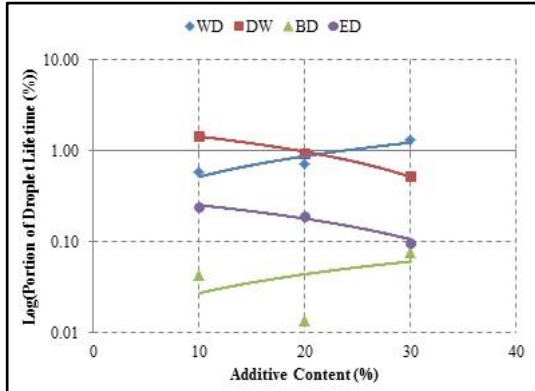
Figure 11: The effect of additive (water, biodiesel, and ethanol) concentration on the net portion of the secondary atomization with respect to the overall droplet lifetime.

Figure 11 represents the ratio of the total period of time (evaluated in μs) where secondary atomization takes place to the total droplet lifetime (also evaluated in μs), to compare the sub-droplet ejection portion with respect to the overall droplet lifetime. The figure has also been presented in the logarithmic form due to the broad difference in magnitudes between the emulsion droplets and those of the blends. As the figure shows, the secondary atomization portion of the droplet lifetime for the BD and ED blends is quite small; in fact it is in the order of $O(10^{-2})$ in the case of the BD blends and $O(10^{-1})$ in the case of the ED blends compared to the overall droplet lifetime. Whereas,

it is in the order of $O(1)$ in the cases of WD and DW emulsions. This suggests that the secondary atomization portion of time represents an infinitesimally small percentage of the overall droplet lifetime. However, this small percentage is important for enhancing fuel evaporation and increasing fuel-air mixing. Thus, increasing this portion of time is important as well. Additionally, as it is discussed above, the figure shows that this portion of time is proportional with the volume fractions of both water and biodiesel in the WD emulsions and BD blends respectively, and is inversely proportional to the volume fractions of water and ethanol in the DW emulsions and ED blends respectively.
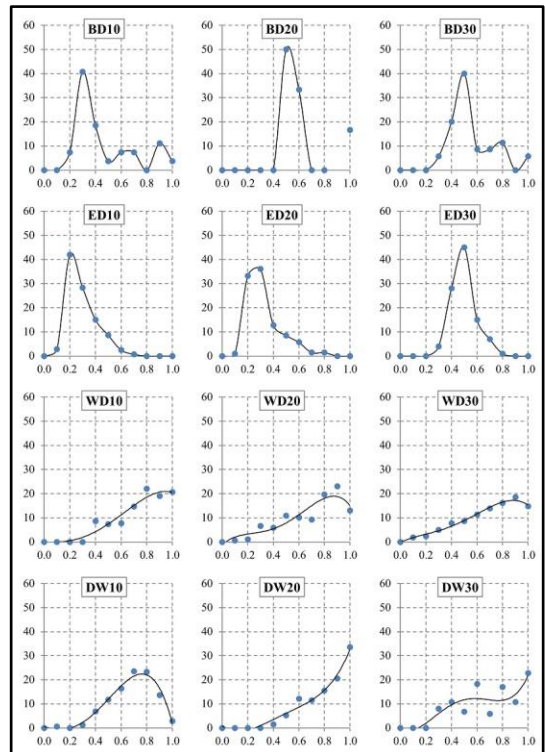
Figure 12: Sub-droplet ejection probability (%) – y-axis – with respect to the normalized droplet lifetime – x-axis – for biodiesel/diesel blends (1st row), ethanol/diesel blends (2nd row), water-in-diesel emulsions (3rd row), and diesel-in-water emulsions (4th row).

Furthermore, in spite of its small percentage in the droplet lifetime, secondary atomization of the multicomponent fuel droplet is found to occur at certain intervals of this lifetime. Hence, these intervals may represent the best occurrence probability for droplet secondary atomization of each fuel. Thus, Figure 12 shows the secondary atomization occurrence probability with respect to the droplet lifetime for all the multicomponent fuel mixtures under investigation. Generally, the figure shows that each of the four mixtures is following a certain atomization trend that is different from the other mixtures. And that this trend is responsive to the increase of the additive in that mixture. For the

biodiesel/diesel blends shown in the first row of Figure 12, it can be seen that the droplet secondary atomization is more likely to start after the first 20% of the droplet lifetime after the heating up period. And that its maximum occurrence probability is shifting from the early 30% for BD10 forwards to midterm the droplet lifetime for the BD20 and BD30 blends. This suggests that the peak sub-droplet population is increasing with increasing the biodiesel concentration in the blends. This sub-droplets proportionality with concentration is shown also in the case of the ethanol/diesel blends in the second row of Figure 12. For these blends, the secondary atomization is shown to take place after the first 10% of the droplet lifetime, so it is slightly earlier than that of BD blends. This trend is in agreement with what is found by Miglani, Basu, and Kumar [12] for bubble generation within the ethanol multicomponent mixtures. The third row of Figure 12 shows the secondary atomization occurrence probability for the water-in-diesel emulsions. Secondary atomization in this mixture is slightly different from those of the BD and ED blends. It starts at after the first 10% of the droplet lifetime and continues to increase with time until reaching its peak slightly before the end of the droplet lifetime. This is the same trend as those of the diesel-in-water emulsion droplets shown in the fourth row. This continuous increase in secondary atomization indicates the high degree of nucleation within the liquid-phase of the droplet compared to the blends, especially when the droplet diameter decreases with time. This is in agreement with the onset rate distribution of secondary atomization obtained by Tsue et. al., [21] for n-dodecane/water and n-tetradecan/water emulsions. Figure 12 shows also that except the probability shift shown in the blends, the concentration of the additive (water, biodiesel, and ethanol) have no effect on the secondary atomization occurrence probability along the droplet lifetime. However, for the samples analysed, the starting time of secondary atomization is shown to be responsive to the concentrations.
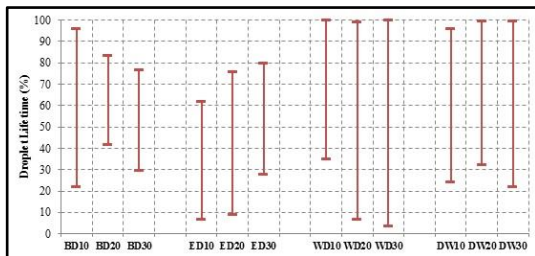
**Figure 13:** The portion of total secondary atomization period compared to the overall droplet lifetime.

This is illustrated clearly in Figure 13 which demonstrates the total interval of time between the first and final occurrences of droplet secondary atomization for all the multicomponent fuel mixtures under investigation. This figure gives an overview about the sub-droplet emission trend for every fuel. From the figure it can be seen that the emulsion fuel droplets are experiencing secondary atomization along almost the whole period of their lifetimes, whereas secondary atomization of the blend fuel droplets constitutes half of that period in average. This is attributed to the higher nucleation rate within the liquid-phase of the emulsion droplets compared to that of the blend droplets. Furthermore, it can be noticed from Figure 13 that the secondary atomization in the emulsion droplets almost lasts to the end of the droplet lifetime. This is because the emulsion droplets usually do not undergo complete evaporation; instead droplet microexplosion takes place fragmenting the droplet into smaller size sub-droplets. This phenomenon did not occur during the combustion of the biodiesel/diesel and ethanol/diesel blends, so that secondary atomization from the droplets of these mixtures does not last to the end of the droplet lifetime. This emulsion droplet microexplosion has been further investigated in the next section for acquiring more insight information to help comprehending this phenomenon that is associated to the combustion of the emulsion fuel droplets.

1.3.2 Liquid-Phase of the Multicomponent Fuel Droplets

In contrast to the single-component fuel droplets, the multicomponent fuel droplets have a less transparent structure. This transparency is variable between the different multicomponent mixtures utilized in the present work. The biodiesel/diesel blends have the highest transparency compared to the other mixtures, then, it comes the ethanol/diesel mixtures, and finally the emulsions of both types the water-in-diesel and diesel-in-water. This is related to the miscibility of biodiesel, ethanol, and water in diesel, where, the biodiesel that is the most miscible liquid in diesel among the three have the most homogeneous – and in turn most transparent – mixture when blended with diesel compared to ethanol and water. Ethanol, on the other hand, is partially miscible as formerly explained. Hence, the resulting ethanol/diesel mixture is less homogeneous and less transparent compared to biodiesel. While, the water/diesel emulsions have a relatively opaque structure compared to the biodiesel and ethanol blends, that is due to the immiscible nature of water in diesel, even with the use of the emulsifying agent. In addition to the difference in transparency, the multicomponent fuel mixtures differ from each other in the nucleation rate and subsequent liquid-phase dynamics. The biodiesel/diesel blend droplets are characterized by steady, undisturbed combustion, with the least nucleation and bubble generation incidents among all the mixtures. Whereas, the ethanol/diesel blends, water-in-diesel-

emulsions, and diesel-in-water emulsions are characterized by chaotic combustion behaviours due to the high nucleation and bubble generation incidents leading to increased puffing and sub-droplet generation values. These chaotic behaviours are reflected on the shape of the burning droplet as shown in Figure 14.
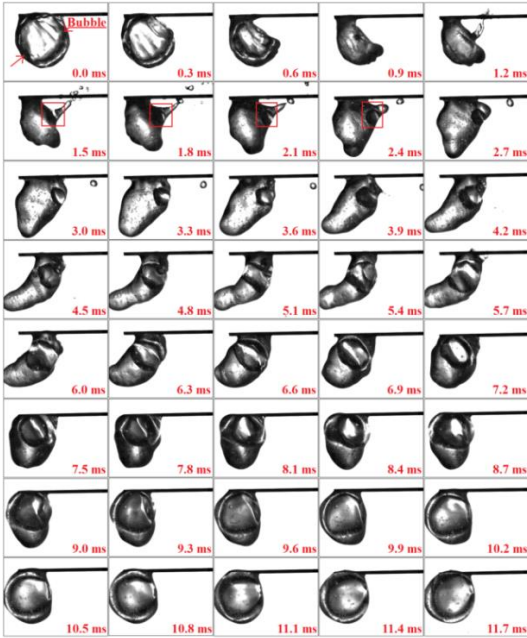

Figure 14: Temporal sequence of the droplet shape variation consequent to bubble burst and puffing within a WD20 fuel droplet (the time is set from the start of puff).

The droplet in the figure endures high deformations in shape subsequent to the puffing incident. Additionally, it experiences all the possible processes subsequent to bubble growth and burst, therefore, it serves as an ideal model for describing these processes. The droplet is initially spherical and contains a large bubble with a diameter equals to 90% of the droplet instantaneous diameter so that it is occupying a large space inside the droplet as shown in the image corresponding to time 0.0 ms in Figure 14. When the bubble bursts, the droplet starts to flatten on the right side as shown in the images corresponding to times 0.3 ms to 0.9 ms respectively. This flattening is a result of the droplet reaction to the thrust force generated during the water vapour release by puffing. The puffing vapour could not be visualized using backlighting because of the high intensity illumination light used for the backlighting imaging. This illumination light is required to compensate for the high speed imaging, but, unfortunately, the too bright background generated by illumination obscures the visualization of the low intensity vapour emitted by puffing. Subsequent to puffing, some of the liquid is ejected outside the droplet accompanied by the detachment of different size ligaments in the form of sub-droplets as shown in images 1.2 ms to 2.4 ms

respectively. The thrust force resulting from puffing then pushes the droplet to the left side so that it takes a plum shape rather than its original spherical (or semi-spherical) shape, as shown in times 2.7 ms to 3.3 ms in the figure. The droplet then continues to move towards the left side under the puffing thrust force, but, the surface tension of the liquid will resist this movement and keep the droplet suspended in the fibre, causing the droplet to elongate at its far end as shown in times 3.6 ms to 5.7 ms respectively. This droplet elongation continues until the surface tension force exceeds the thrust force and brings the droplet back to its normal position (times 6.0 ms to 7.2 ms respectively) and shape (times 7.5 ms to 11.7 ms). This sequence of events occurs almost after every bubble growth and burst processes but with varying intensity, because not all bubble burst processes end up with ligament or sub-droplet detachment. Furthermore, as shown in image 1.5 ms and the following images, another bubble is generated in the ejection location subsequent to ligament and sub-droplets detachment. Direct connection between the ejection site and the evolution of the new bubble could not be confirmed. Despite the reasons behind this bubble generation, it gives an indication of the nucleation and bubble growth rates in the emulsion droplets. Moreover, Figure 14 shows the variety of shapes taken by the droplet during a single occurrence of secondary atomization. Hence, keeping in mind the repeatability of such process, especially for the emulsion droplets, it can be inferred how dominant is the irregular shape of the droplet compared to the regular spherical configuration.

1.3.3 Nucleation Rate

In spite of the size – and the resulting time scale – difference between the tested droplets in the present work and those on the real sprays, the nucleation behaviour of the different multicomponent fuels under investigation could be estimated. Hence, the nucleation rates during the droplet combustion of these fuels have been evaluated and presented in Figure 15 with respect to the concentration of the added substance (biodiesel, ethanol, or water). These nucleation rates have been evaluated for the overall droplet lifetime and normalized by 100 ms time interval for procuring more realistic results comparable to the real spray droplet lifetime. Additionally, the nucleation rate has been presented in the logarithmic form due to the large difference in the order of magnitude of the computed values for the different multicomponent fuel mixtures. Bubble nucleation around the fibre region inside the droplet is neglected to eliminate the probability of adding any bubble generated by heterogeneous nucleation due to the presence of the fibre.

11
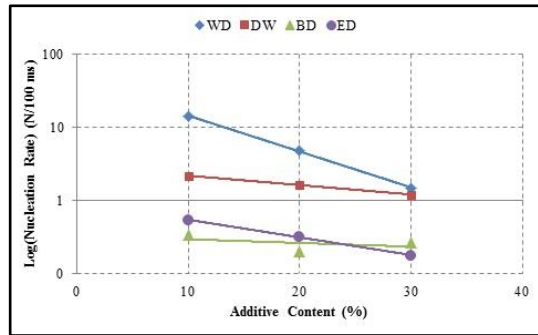
Figure 15: Average nucleation rate variation with the content of the substance added to diesel.

Hence, the presented results are only for homogeneous nucleation away from the fibre. As shown in the figure, the nucleation rates of all the investigated mixtures are inversely proportional to the concentration of the additive in that mixture. However, the degree of this proportionality is variable among those mixtures. Where, the water-in-diesel emulsions show steep line behaviour with increasing the concentration of the water in the emulsions, whereas this behaviour is less for the other mixtures. Additionally, the nucleation rate in the WD emulsions is the highest among all mixtures, while that of the BD blends is the least, this could be a reflection to the miscibility of these liquids to diesel, where biodiesel is completely miscible and water is completely immiscible.
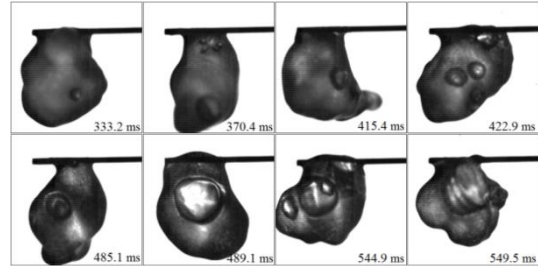

Figure 16: Different nucleation sites inside the burning fuel droplet.

Figure 16 shows the various nucleation sites inside a WD10 emulsion droplet. The figure shows that the nuclei could initiate at any location inside the droplet, whether this location is the droplet centre as in image 489.1 ms, or any of the peripheries, as it is shown in the other images. All these nucleation sites are away from the suspension fibre, which gives certainty about the occurrence of homogeneous nucleation within the burning multicomponent fuel droplet. Furthermore, the figure shows that more than one nucleus may develop at the same time, as it is revealed in images 422.9 ms and 544.9 ms.

1.3.4 Bubble Dynamics

Once the nucleation rate has been evaluated, the resulting bubble growth and dynamics are

investigated. Figure 17 shows the bubble growth rate (BGR) in (μm^3/μs) inside the burning droplets of the multicomponent fuels under investigation presented with respect to the concentration of the substance added to diesel (biodiesel, ethanol, and water). The growth rate is expressed in the logarithmic form due to the large difference between the mixtures.
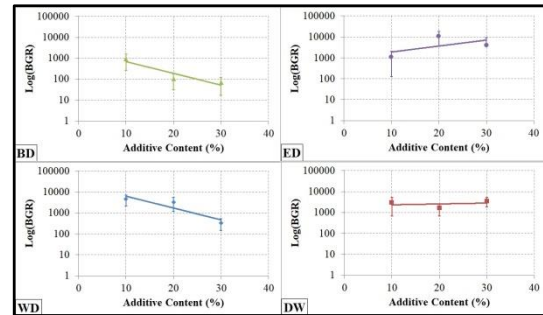
**Figure 17:** The effect of additive content on the bubble growth rate inside the multicomponent fuel droplet.

As Figure 17 shows, the bubble growth rate of ethanol/diesel blends is proportional to the increase of ethanol concentration in the blend, while, those growth rates of both biodiesel/diesel blends and water-in-diesel emulsions are inversely proportional to the increase in both biodiesel and water concentrations in the mixture. The bubble growth rate of the diesel-in-water emulsions on the other hand is found to be unaffected by the increase of water concentration in the emulsion.
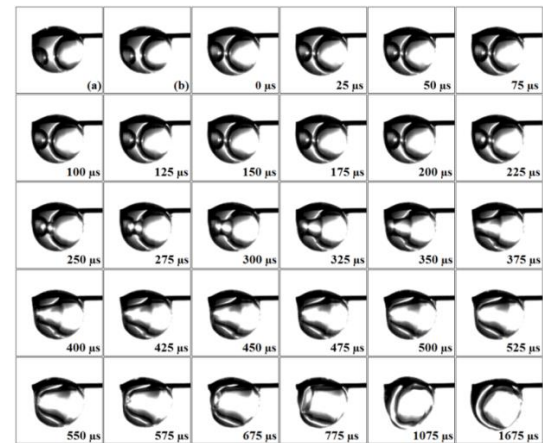
Figure 18: Temporal sequence of two bubbles merging occurrence inside an ED10 fuel droplet (time is set from the instant of bubbles attachment).

Furthermore, more than one bubble could be initiated at the same – or relatively close – time. Hence, some of these bubbles are shown to merge into a single large bubble as shown in Figure 18. In this figure, two different size bubbles generated during the combustion of ED10 fuel droplet are united in one large bubble occupying the whole droplet interior. The time periods shown in the figure are set to start from the instant when the two

12

bubbles are attaching each other. However, the first two images in the first row of the figure are before that time, but they have been added to illustrate the change in bubble locations inside the droplet. As the figure shows, the smaller bubble is contained by the larger droplet. This bubble merging process has occurred in many occasions and within different fuel droplets. These merging incidents are playing a crucial rule in the dynamics of the droplet surface since these processes unite multiple small bubbles in one large bubble; the explosion of this large bubble is expected to be more effective than the initial smaller ones. However, the larger bubble size will not necessarily generate the sufficient disturbance for disintegrating the droplet. Since the bubble size is not the only effective parameter in droplet disintegration and sub-droplet generation, the other factors are droplet size, bubble location prior to burst [33], and droplet liquid surface tension [34].
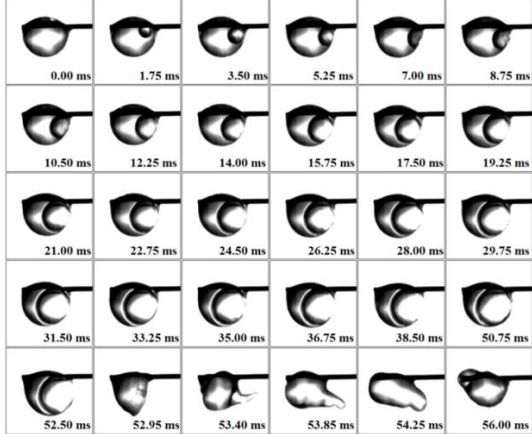
Figure 19: Temporal sequence of bubble growth inside a burning BD10 fuel droplet.

Figure 19 shows the temporal sequence of bubble growth inside a burning BD10 fuel droplet. The presented bubble has initiated near the droplet surface and developed in the same location as shown in image 3.50 ms and the followings. Its diameter on image 52.50 ms prior to explosion is measured to be 0.73 of the droplet diameter. However, when exploded, its effect on the droplet is only shown in the form of vapour ejection by puffing without detachment of any portion of the liquid droplet as shown in image 53.40 ms and following images. This suggests that the thrust force resulted from bubble explosion and the subsequent puffing was not sufficiently high to overcome the surface tension of the liquid droplet. Especially, the surface tension of the biodiesel fuels is higher than that of the regular diesel fuels [35]. So that its only effect appeared in the form of droplet shape change followed by restitution to the normal shape.
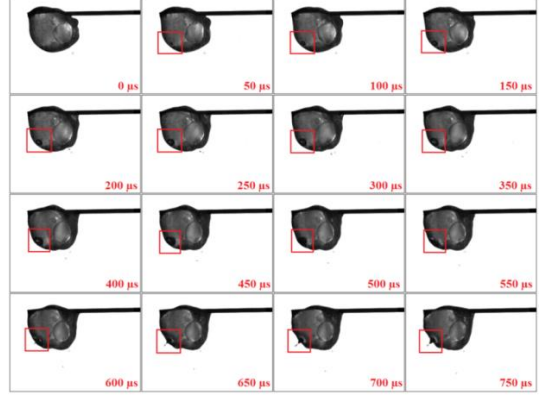

Figure 20: Short bubble growth time during the combustion of WD20 fuel droplet.

In contrast, Figure 20 shows bubble evolution and explosion inside a WD20 fuel droplet, in which this explosion led to sub-droplet detachment from the parent droplet surface. The bubble is also initiated near the surface of the droplet as shown in image 50 µs, and developed adjacent to the surface as shown in images 100 µs to 550 µs respectively. Its maximum diameter prior to burst is estimated from image 550 µs to be 0.28 of the droplet diameter, and its evolution time is 1/95 of the evolution time for that bubble shown in Figure 19. However, its explosion led to the generation of small size sub-droplet as shown in image 750 µs. Thus, it can be inferred that the size of the bubble is not always the major factor in deciding the occurrence of droplet secondary atomization.

1.3.5 The Effect of Bubbles on Puffing, Secondary Atomization, and Microexplosion

Figure 21 shows the effect of bubble burst on the sub-droplet ejection from the surface of an ED20 fuel droplet undergoing combustion. Prior to burst, the bubble – bounded by the red box in the first row – is adjacent to the droplet surface. Hence, it is forcing the frontal thin liquid layer of the liquid until it is in contact with the gaseous environment. So, the pressure difference across the bubble causes its rapture releasing all the content vapour outside. The release of this vapour created a low pressure spot on the droplet surface causing the surrounding liquid on the droplet to flow towards this spot as shown in images 0.05 ms to 0.45 ms in Figure 21. These images illustrate the inward movement of the droplet surface subsequent to vapour release by bubble rapture. This inward motion of the liquid edges results in a reflective outward motion of part of the liquid due to the impact of the liquid edges in the low pressure spot as shown in image 0.45 ms and the followings. If the force resulting from this reflective motion is high enough, the moving liquid portion will continue forward with a decrease in the cross-sectional area and flattening in the upstream

side as shown in images 0.85 ms to 0.95 ms. With the increase of outward motion of the liquid, the cross-sectional area decrease and upstream face increase will initiate nicking in the liquid portion structure behind the flattened face as shown in the red circles of images 1.00 ms to 1.20 ms.
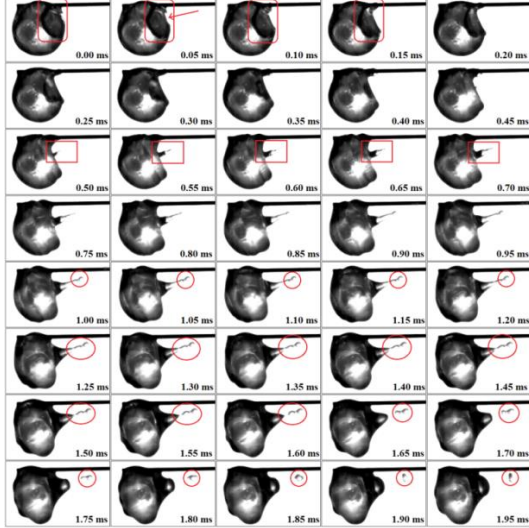
Figure 21: Temporal sequence of the effect of a growing bubble on the sub-droplet ejection from an ED20 droplet.

Disintegration of the liquid from this nick then occurs causing a small ligament of liquid to escape in the form of sub-droplet as shown in images 1.25 ms to 1.95 ms respectively. Otherwise, if the force produced by the impact is not sufficiently enough, liquid nicking will not take place, and the resulting effect will be limited to instantaneous deterioration of the droplet surface for a certain time after which the droplet will retain its original shape as it is previously shown in Figure 19.

The above described synopsis occurs for all the growing bubbles inside the fuel droplets, but with varying degree. Where, occasionally the impact force is relatively small due to the small size of the exploding bubble and in turn the low pressure difference. Hence, smaller portion of the liquid is forced outside as shown in Figure 22. This figure illustrates the temporal sequence of bubble growth inside a WD20 fuel droplet. As it is shown by tracking the bubble bounded by the red box in each image, the bubble is initiated at time 181.1 ms near the droplet surface. Then, it continued to grow up with time until reaching the instant 183.1 ms where it reached its maximum size and attached the droplet surface from inside. Since, the liquid layer at the droplet surface is thin; it did not withstand the force exerted by the bubble. Therefore, droplet surface layer rupture occurred bringing the bubble in contact with the surrounding gaseous environment. This attachment with the environment led to the rapture of the bubble itself due to the pressure difference across the bubble boundaries.
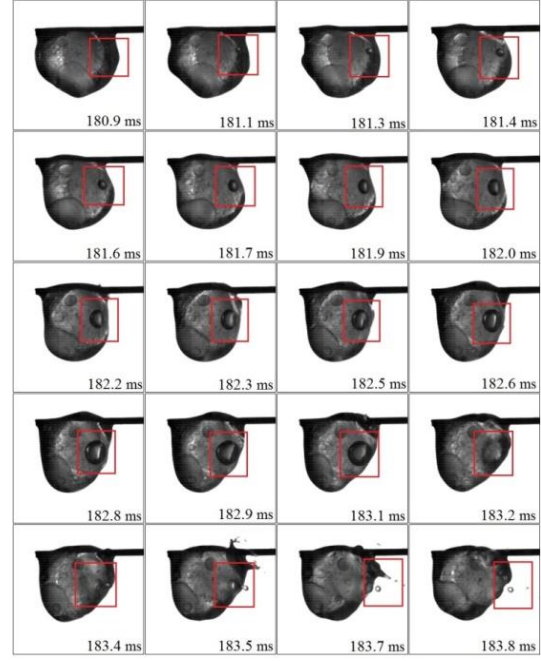
Figure 22: Temporal sequence of the effect of a growing bubble on the sub-droplet ejection from a burning WD10 fuel droplet.

Because of this rapture, a small portion of the liquid from the droplet surface is ejected according to the same mechanism described formerly. However, this liquid portion is relatively small as shown in images 183.5 ms to 183.8 ms.
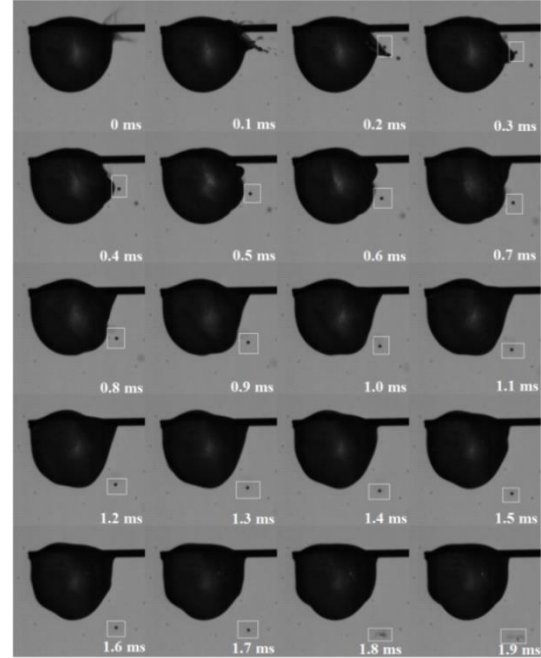
Figure 23: Temporal sequence of the ejected sub-droplet lifetime during the combustion of a WD20 fuel droplet.

Figure 23 on the other hand, shows the secondary atomization and sub-droplet emission from a WD20 fuel droplet. The sub-droplet is bounded by the white rectangle for tracking purposes. It is emitted as a result of the parent

droplet puffing shown in images at 0 ms and 0.1 ms. Although the exact composition of the sub-droplet is not currently affordable; its burning characteristics are compared to the parent droplet that is WD20. The initial diameter of the sub-droplet is found to be 40 μm. It has experienced explosion at about 1.9 ms after its ejection. Therefore, its burning rate constant is calculated as (0.84 mm^2/s), which is slightly lower than the (1.18 mm^2/s) of the WD20 fuel droplet. Though, in the case of sub-droplet, this value represents the vaporization rate constant rather than the burning rate constant since the sub-droplet experienced explosion before leaving the vaporization zone of the parent droplet. Since the radial distance of the sub-droplet centre from the parent droplet centre in image 1.8 ms is evaluated to be 1.8 of the parent droplet instantaneous radius. Whereas, the flame stand-off ratio for that droplet is found to be ~ 4. Thus, the sub-droplet is more likely to explode during vaporization rather than combustion. This implies that the actual secondary atomization from the emulsion droplet is higher than that estimated from the regular droplet and flame observations.
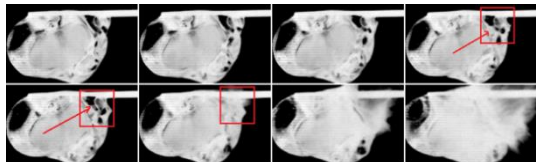

Figure 24: WD20 emulsion fuel droplet microexplosion (the time difference between images is 25μs).

Figure 24 shows the temporal sequence of WD20 emulsion fuel droplet microexplosion during combustion. The images have been inverted using Matlab for proper visualization of the explosion initiation point. The use of high intensity backlight during imaging resulted in the tracking of the explosion point inside the droplet is quiet challenging. As the figure reveals, the micro-explosion of the droplet took place due to the explosion of one of the bubbles inside the droplet. This bubble – bounded by the red box –exploded inside the droplet in a point relatively far away from the droplet surface. Hence, due to its location inside the droplet, the effect of this explosion on the droplet was more intensive than the bubble explosions on the droplet surface. This form of microexplosion has been noticed to occur during the combustion of the majority of the water-in-diesel and diesel-in-water emulsion droplets and for some of the ethanol/diesel blends.

1.3.6 Accumulation within the Burning Multicomponent Fuel Droplet

During the liquid-phase magnified monitoring throughout the combustion of the multicomponent fuel droplets, some of the droplets belonging to the ethanol/diesel blends, water-in-diesel and diesel-in-water emulsions have experienced a kind of component separation. This is followed by accumulation of one of these components in the form of a spherical mass moving in the centre of the droplet as shown in Figure 25. As the figure shows, the structure and transparency of this mass are different from those of the bubble. Hence, it implies that the formation of this mass is due to the separation of the components of the fuel mixture and the distillation of the less volatile component in the centre of the droplet. In the case of the ethanol/diesel blends, the less volatile component in the blend is the diesel, thus, the mass accumulating in the centre of the droplet in Figure 25 is expected to be diesel.
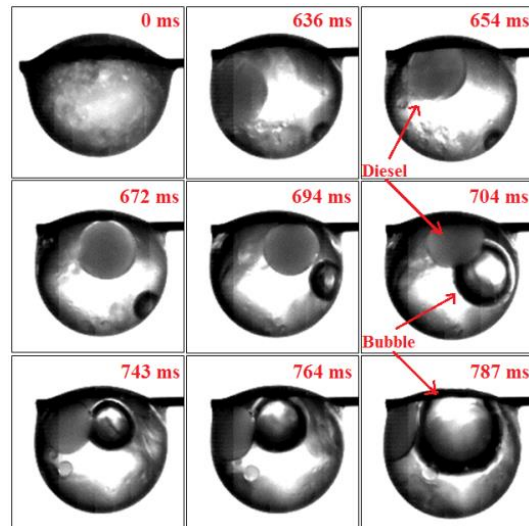
Figure 25: Diesel fuel distillation during the combustion of ED30 fuel droplet.
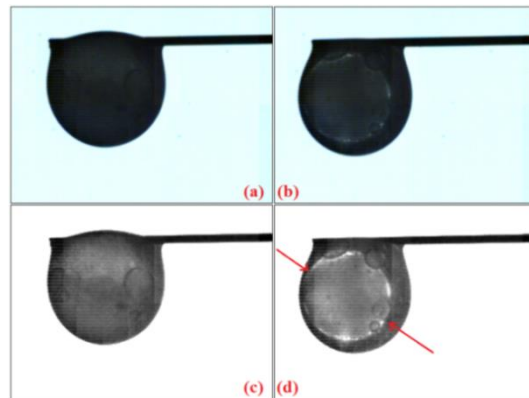
Figure 26: Water distillation during the combustion of WD20 fuel droplet: (a) original image at time =0, (b) original image with water distillation appears in the middle, (c) intensity enhanced (a) image, and (d) intensity enhanced (b) image.

This is also shown in Figure 26 for the combustion of WD20 fuel droplet. For both water-in-diesel and diesel-in-water emulsions water is the less volatile component, hence, the accumulating mass in Figure

26 is expected to be water rather than diesel. This distilled water is shown to augment the nucleation and bubble generation rates inside the droplet because it serves as a nucleation site. This type of separation and distillation has not been noticed to occur during the combustion of biodiesel/diesel blends, which may be attributed to the complete miscibility of biodiesel in diesel as explained formerly.

1.4 Conclusions

In the present work, a magnified high speed imaging of the liquid-phase during the droplet combustion of the multicomponent fuels have been performed. Several physical processes have been visualized and tracked including nucleation, bubble generation, and fuel component separation and accumulation. Quantitative analysis has been performed for estimating the nucleation and bubble growth rates.

The high speed images have revealed the occurrence of homogeneous nucleation within the multicomponent fuel droplet during combustion. The subsequent analysis then, have shown that the rate of this nucleation is inversely proportional to the degree of miscibility between the basic constituents of the multicomponent fuel mixture. Thus, the biodiesel/diesel blends – which are the mixtures of the completely miscible components – are characterized with the least nucleation rates, whereas the water/diesel emulsions – which are the mixtures with the least miscibility of components among all the studied mixtures – have had the highest nucleation rates.

The effect of nucleation and bubble generation on the puffing, secondary atomization, and microexplosion of the multicomponent fuel droplet has also been investigated. It is shown that the size of the bubble is not the only factor that determines sub-droplet emission from the droplet surface.

Additionally, some bubble dynamics have also been observed, such as the bubble circulation and the multiple bubble merge. All these processes have an effect on the overall dynamics of the droplet liquid-phase and surface during combustion.

Furthermore, separation and accumulation of diesel in the ethanol/diesel blends, and water in the water-in-diesel and diesel-in-water emulsions has been observed. This accumulation leads to the generation of a relatively large size mass in the centre of the droplet; this mass sometimes serves as a nucleation site resulting in increasing the nucleation rate within the droplet.

Although the tests have been performed on large droplets, the present findings can be used for giving a general description of each of the processes studied. These in turn, serve as a basis for future work on spray combustion characteristics of the multicomponent fuels.

References

[1] Warnatz, J., Maas, U., Dibble, R.W. "*Combustion: Physical and Chemical Fundamentals, Modeling and Simulation, Experiments, Pollutant Formation.*" 4th Editio. Springer; 2006.

[2] Lefebvre, A.H. "*Atomization and Sprays.*" Hemisphere Publishing Corporation; 1989.

[3] Wang, C. H., Liu, X. Q., Law, C.K. "*Combustion and Microexplosion of Freely Falling Multicomponent Droplets.*" Combustion and Flame 1984;56:175–97.

[4] Siringnano, W.A. "*Fluid Dynamics and Transport of Droplets and Sprays.*" 2nd Editio. Cambridge University Press; 2010.

[5] Takei, M., Tsukamoto, T., Niioka, T. "*Ignition of Blended-Fuel droplet in High-Temperature Atmosphere.*" Combustion and Flame 1993;93:149–56.

[6] Botero, M. L., Huang, Y., Zhu, D. L., Molina, A., Law, C.K. "*Synergistic Combustion of Droplets of Ethanol, Diesel and Biodiesel Mixtures.*" Fuel 2012;94:342–7.

[7] Hoxie, A., Schoo, R., Braden, J. "*Microexplosive Combustion Behavior of Blended Soybean Oil and Butanol Droplets.*" Fuel 2014;120:22–9.

[8] Mikami, M., Yagi, T., Kojima, N. "*Occurrence Probability of Microexplosion in Droplet Combustion of Miscible Binary Fuels.*" Symposium (International) on Combustion/The Combustion Institute 1998;27:1933–41.

[9] Shinjo, J., Xia, J., Ganippa, L.C., Megaritis, A. "*Physics of Puffing and Microexplosion of Emulsion Fuel Droplets.*" Physics of Fluids 2014;26:103302.

[10] Tsue, M., Segawa, D., Kadota, T., Yamasaki, H. "*Observation of Sooting Behavior in an Emulsion Droplet Flame by Planar Laser Light Scattering in Microgravity.*" Symposium (International) on Combustion/The Combustion Institute 1996;26:1251–8.

[11] Watanabe, H., Harada, T., Matsushita, Y., Aoki, H., Miura, T. "*The Characteristics of Puffing of the Carbonated Emulsified Fuel.*" International Journal of Heat and Mass Transfer 2009;52:3676–84.

[12] Miglani, A., Basu, S., Kumar, R. "*Insight into Instabilities in Burning Droplets.*" Physics of Fluids 2014;26.

[13] Wang, Z.G. *"Internal Combustion Processes of Liquid Rocket Engines: Modeling and Numerical Simulations."* John Wiley and Sons Ltd.; 2016.

[14] Lasheras, J. C., Fernandez-Pello, A. C., Dryer, F.L. *"Experimental Observations on the Disruptive Combustion of Free Droplets of Multicomponent Fuels."* Combustion Science and Technology 1980;22:195–209.

[15] Lasheras, J. C., Fernandez-Pello, A. C., Dryer, F.L. *"On the Disruptive Burning of Free Droplets of Alcohol/n-Paraffin Solutions and Emulsions."* Symposium (International) on Combustion/The Combustion Institute 1981;18:293–305.

[16] Lasheras, J. C., Yap, L. T., Dryer, F.L. *"Effect of the Ambient Pressure on the Explosive Burning of Emulsified and Multicomponent Fuel Droplets."* Symposium (International) on Combustion / The Combustion Institute 1984;20:1761–72.

[17] Yang, J. C., Avedisian, C.T. *"The Combustion of Unsupported Heptane/Hexadecane Mixture Droplets at Low Gravity."* Symposium (International) on Combustion/The Combustion Institute 1988;22:2037–44.

[18] Jackson, G. S., Avedisian, C.T. *"Combustion of Unsupported Water-in-n-Heptane Emulsion Droplets in a Convection-Free Environment."* International Journal of Heat and Mass Transfer 1998;41:2503–15.

[19] Liu, Y. C., Avedisian, C.T. *"A Comparison of the Spherical Flame Characteristics of Sub-Millimeter Droplets of Binary Mixtures of n-Heptane/Iso-Octane and n-Heptane/Toluene with a Commercial Unleaded Gasoline."* Combustion and Flame 2012;159:770–83.

[20] Chung, S. H., Kim, J.S. *"An Experiment on Vaporization and Microexplosion of Emulsion Fuel Droplets on a Hot Surface."* Symposium (International) on Combustion / The Combustion Institute 1990;23:1431–5.

[21] Tsue, M., Yamasaki, H., Kadota, T., Segawa, D., Kono, M. *"Effect of Gravity on Onset of Microexplosion for an Oil-in-Water Emulsion Droplet."* Symposium (International) on Combustion/The Combustion Institute 1998;27:2587–93.

[22] Wang, C. H., Fu, S. Y., Kung, L. J., Law, C.K. *"Combustion and Microexplosion of Collision-Merged Methanol/Alkane Droplets."* Proceedings of the Combustion Institute 2005;30:1965–72.

[23] Shinjo, J., Xia, J. *"Combustion Characteristics of a Single Decane/Ethanol Emulsion Droplet and a Droplet Group under Puffing Conditions."* Proceedings of the Combustion Institute 2017;36:2513–21.

[24] Shinjo, J., Xia, J., Ganippa, L. C., Megaritis, A. *"Puffing-Enhanced Fuel/Air Mixing of an Evaporating n-Decane/Ethanol Emulsion Droplet and a Droplet Group under convective heating."* Journal of Fluid Mechanics 2016;793:444–76.

[25] Mollet, H., Grubenmann, A. *"Formulation Technology: Emulsions, Suspensions, Solid Forms."* Wiley-VCH; 2001.

[26] Tadros, T.F. *"Emulsion Science and Technology."* Wiley-VCH; 2009.

[27] Griffin, W.C. *"Classification of Surface-Active Agents by HLB."* Journal of Cosmetic Science 1949;1:311–26.

[28] Califano, V., Calabria, R., Massoli, P. *"Experimental Evaluation of the Effect of Emulsion Stability on Micro-Explosion Phenomena for Water-in-Oil Emulsions."* Fuel 2014;117:87–94.

[29] Yap, L., Kennedy, I. M., Dryer, F.L. *"Disruptive and Micro-Explosive Combustion of Free Droplets in Highly Convective Environments."* Combustion Science and Technology 1984;41:291–313.

[30] Xu, Y., Keresztes, I., Condo, A. M., Phillips, D., Pepiot, P., Avedisian, C.T. *"Droplet Combustion Characteristics of Algae-Derived Renewable Diesel, Conventional #2 Diesel, and their Mixtures."* Fuel 2016;167:295–305.

[31] Roesle, M. L., Kulacki, F.A. *"Boiling Heat Transfer in Dilute Emulsions."* Springer; 2013.

[32] Colbeck, I. Aerosol Formation. In: Wedlock DJ, editor. Controlled Particle, Droplet and Bubble Formation, Butterworth-Heinemann; 2004, p. 137–58.

[33] Shinjo, J., Xia, J., Umemura, A. *"Droplet/Ligament Modulation of Local Small-Scale Turbulence and Scalar Mixing in a Dense Fuel Spray."* Proceedings of the Combustion Institute 2015;35:1595–602.

[34] Shinjo, J., Umemura, A. *"Droplet/Turbulence Interaction and Early Flame Kernel Development in an Autoigniting Realistic Dense Spray."* Proceedings of the Combustion Institute 2013;34:1553–60.

[35] Shehata, M. S., Abdel Razek, S.M. *"Experimental Investigation of Diesel Engine Performance and Emission Characteristics using Jojoba/Diesel Blend and Sunflower Oil."* Fuel 2011;90:886–97.